Acta Cryst. (1997). D**53**, 650–657

X-ray Structure of Turkey-Egg Lysozyme Complex with Tri-*N*-acetylchitotriose. Lack of Binding Ability at Subsite *A*

KAZUAKI HARATA* AND MICHIRO MURAKI

National Institute of Bioscience and Human Technology, 1-1 Higashi, Tsukuba, Ibaraki 305, Japan.
E-mail: harata@nibh.go.jp

(*Received 23 October 1996; accepted 8 April 1997*)

Abstract

The turkey-egg lysozyme (TEL) complex with tri-*N*-acetylchitotriose [$(GlcNac)_3$] was co-crystallized from 1.5% TEL and 2 m*M* $(GlcNac)_3$ at pH 4.2. The crystal structure was determined by molecular replacement and refined to an *R* value of 0.182 using 10–1.77 Å data. The $(GlcNac)_3$ molecule occupies the subsites *A*, *B* and *C*. At the subsites *B* and *C*, the sugar residues are bound in a similar manner to that found in the hen-egg lysozyme (HEL) complex. In contrast, the GlcNac residue at the subsite *A* is exposed to bulk solvent and has no contact with the protein molecule because the active residue Asp101 in HEL is replaced by Gly in TEL. A sulfate ion is bound in the vicinity of subsite *B* and forms hydrogen bonds with the sugar residue and the guanidino group of Arg61, assisting the binding of the sugar residue to subsite *B*. The active-site cleft of TEL is narrower than that of native TEL, thus attaining the best fit of the $(GlcNac)_3$ molecule. The lack of binding ability of subsite *A* is discussed in relation to the catalytic properties of TEL. The result suggests that the cleavage pattern of oligosaccharide substrates in the catalytic reaction is regulated by the protein–sugar interaction at subsite *A*.

1. Introduction

Turkey-egg lysozyme (TEL) belongs to the same class as hen-egg lysozyme (HEL) and differs in seven of the 129 amino-acid residues from HEL (LaRue & Speck, 1970). Compared with HEL, the most important amino-acid replacement with respect to the catalytic activity is found at residue 101, which is Gly in TEL but Asp in HEL. The active site of HEL consists of six subsites designated *A* to *F* (Blake *et al.*, 1967). The Asp101 residue of HEL is located at the subsite *A* and forms hydrogen bonds with the substrate sugar. The catalytic property of TEL is similar to that of HEL; however, distinct differences have been observed which have been ascribed to the replacement of residue 101. The binding ability of HEL for oligosaccharides differs between pH 2.0 and 5.0; HEL binds the saccharide more strongly at pH 5.0 (Banerjee & Rupley, 1975). In contrast, no pH dependence of sugar binding has been observed for TEL in the corresponding pH range (Arnheim, Millet & Raftery, 1974). In the hydrolysis of penta-*N*-acetylchitopentaose $[(GlcNac)_5]$, HEL produces *N*-acetylglucosamine (GlcNac) as a major product. On the other hand, TEL produces much more di-*N*-acetylchitobiose $[(GlcNac)_2]$ than GlcNac (Fukamizo, Torikata, Nagayama, Minematsu & Hayashi, 1983; Fukamizo, Hayashi & Goto, 1986).

The crystallization of TEL was first reported by LaRue & Speck (1970) and a crystallographic study was reported by Bott & Sarma (1976). The three-dimensional structure of the hexagonal crystal was solved at 2.5 Å resolution by Howell, Almo, Persons, Hajdu & Petsko (1992). We have found that TEL crystallizes in a monoclinic form, space group $P2_1$; its structure was determined at 1.3 Å resolution (Harata, 1993). In a previous paper, we reported that TEL binds to the α anomer of $(GlcNac)_2$ in a manner not assumed in the catalytic reaction (Harata & Muraki, 1995). In this paper, we present the crystal structure of the TEL complex with tri-*N*-acetylchitotriose $[(GlcNac)_3]$ and compare it with the structure of the HEL complex with $(GlcNac)_3$, in which the sugar occupies the subsites *A*, *B* and *C* (Cheetham, Artymiuk & Phillips, 1992). Compared with HEL, the 101st residue at subsite *A* is replaced by Gly in TEL. The structural comparison of the sugar complexes with HEL and TEL will provide information pertinent to the elucidation of the difference in the catalytic properties.

2. Materials and methods

2.1. *Crystallization and data collection*

The crystal of the 1:1 complex of TEL with $(GlcNac)_3$ was prepared at pH 4.2 from a 2.2 *M* ammonium sulfate solution containing 10% 1-propanol, 1.5% protein and 2 m*M* $(GlcNac)_3$, according to a procedure previously used for the preparation of the native crystal (Harata, 1993). Thin needles belong to the space group *C*2, with $Z = 4$ and cell dimensions $a = 87.49$, $b = 32.94$, $c = 49.00$ Å and $\beta = 119.1°$. Intensity data were collected up to 1.77 Å resolution on an Enraf–Nonius FAST diffractometer equipped with an Elliott GX21 generator (40 kV, 60 mA, focal spot size 0.3 × 3 mm). Two crystals

with approximate dimensions 0.1 × 0.3 × 0.8 mm were used for data collection and 50 234 measured reflections ($F > 0$) were reduced to 10 950 independent reflections, with an R_{merge} value of 0.058 (86% completeness).

2.2. *Structure determination and refinement*

The structure of the TEL complex with $(GlcNac)_3$ was solved by the molecular-replacement method using the program *X-PLOR* (Brünger, 1992). The cross-rotation search was performed on the Patterson map calculated with the 15–4 Å resolution data. The structure of the native TEL was used as a search model and vectors in the range 5–20 Å were selected. The 191 solutions obtained were subjected to PC refinement, which gave a single plausible solution given by Eulerian angles $(\theta_1, \theta_2, \theta_3) = (88.8, 56.4, 270.5°)$. The position of the molecule in the unit-cell was determined by the translational search. The structure model with the highest correlation gave an R value of 0.32 for the 8–3.5 Å data.

The structure was refined by energy minimization combined with simulated annealing (Brünger, Kuriyan & Karplus, 1987) using reflections with $F_o > 2\sigma(F)$ in the resolution range 10–1.77 Å. $(GlcNac)_3$, water molecules and a sulfate ion were picked on $2F_o - F_c$ and $F_o - F_c$ maps. Water peaks higher than 3σ on the $F_o - F_c$ map were taken into account but those with B values greater than 60 Å^2 were rejected during the refinement. The final model included a TEL molecule, a $(GlcNac)_3$ molecule, a sulfate ion and 85 water molecules. Atomic coordinates and structure factors have been deposited with the Protein Data Bank, Brookhaven National Laboratory.†

3. Results

3.1. *Crystallization*

Crystals of the TEL complex with $(GlcNac)_3$ were prepared by co-crystallization. An attempt to soak $(GlcNac)_3$ into the native TEL crystal was unsuccessful because the crystal rapidly dissolved in the presence of $(GlcNac)_3$. The TEL–$(GlcNac)_3$ complex crystallized in space group $C2$, differing from that ($P2_1$) of the native TEL crystal (Harata, 1993).

3.2. *Structure determination and refinement*

The structure was determined by the molecular-replacement method and refined using *X-PLOR* to an R value of 0.182 ($R_{free} = 0.225$) for 9911 reflections (82% completeness) with $F_o > 2\sigma(F)$ in the resolution range 10–1.77 Å. The final structure model included a TEL molecule, a $(GlcNac)_3$ molecule, a sulfate ion and 85 water molecules. The coordinate error estimated from the Luzzati plot was *ca* 0.2 Å (Luzzati, 1952). The (φ,ψ) angles fall within the normal values on the Ramachandran map. The r.m.s. deviations of bond distances and angles from their ideal values were 0.013 Å and 2.7°, respectively.

3.3. *Structure of TEL*

The backbone structure of TEL (Fig. 1) is essentially the same as that of native TEL (Harata, 1993) although some differences were observed in the conformation of the loop regions. Three residues, Arg14, Arg61 and Ser86, were found to be disordered and in each case two different conformers were considered, as shown in Fig. 2. The TEL structure was superimposed on the structure of native TEL and the positional differences of each equivalent C^α atom are plotted in Fig. 3. The r.m.s. deviation of the TEL structure in the complex from the native TEL structure is 0.39 Å. The large deviations are observed in the residue regions 46–48, 67–72 and 100–103: the 46–48 residues form a type I β-turn connecting two β-strands, 41–45 and 50–54; the 67–72 region forms a type II β-turn (69–72 residues), which is not found in native TEL; and the 100–103 residues, including Gly101 instead of Asp101 in HEL, are located at the subsite *A*. This 101–103 region forms a type III β-turn, instead of a type I β-turn in native TEL. The large deviation in the 46–48 region is caused by the accumulation of the

† Atomic coordinates and structure factors have been deposited with the Protein Data Bank, Brookhaven National Laboratory (Reference: 1JEF, R1JEFSF). Free copies may be obtained through the Managing Editor, International Union of Crystallography, 5 Abbey Square, Chester CH1 2HU, England (Reference: TS0004).

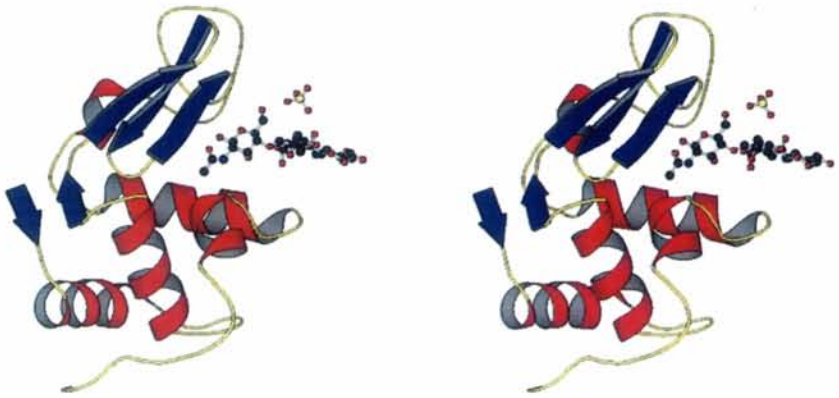

Fig. 1. Stereoview of the structure of the TEL complex with $(GlcNac)_3$ drawn by the program *MolScript* (Kraulis, 1991). The $(GlcNac)_3$ molecule and sulfate ions are shown with circles.

differences of the (φ,ψ) angles of these residues. The largest difference is observed for Thr47: (–69.8,–14.9°) for the complexed TEL and (–41.2,–40.2°) for the native TEL. The average displacement parameter for each residue is plotted in Fig. 4. The average B value for the peptide groups of the molecule is 17.6 Å^2 and that for all atoms of the molecule is 19.2 Å^2. The α-helixes and β-strands have main-chain displacement parameters less than 20 Å^2. On the other hand, the regions having relatively large displacement parameters (except the C-terminal region), 18–22, 45–48, 67–73, 85–87 and 100–103, are found near the surface of the molecule and form loop or β-turn structures.

3.4. *Structure of (GlcNac)$_3$*

Each pyranose ring in the three GlcNac residues, NAG1, NAG2 and NAG3, located at the subsites *A*, *B* and *C*, respectively, takes a normal chair conformation (Figs. 5 and 6). The *N*-acetyl group adopts the same conformation in the three residues and the C8—C7 bond is *trans* to the C2—N2 bond (the numbering of the pyranose ring is shown in Fig. 7). The C6—O6 bond in NAG1 has a (+)-*gauche* conformation with respect to the C5—O5 bond, while a (–)-*gauche* conformation is observed in the other residues. The molecule takes a helically extended form and the conformation of each glycosidic linkage is similar to that observed in the crystal structure of $(GlcNac)_2$ (Mo & Jensen, 1978). The twist angle around the glycosidic linkage was calculated as an angle between the planes through O1, C1, C4 and O4 of each sugar residue. The angles are 34° between NAG1 and NAG2 and 39° between NAG2 and NAG3. The twisted conformation is supported by the O3—H···O5′ inter-residue hydrogen bonds (the distance is 2.7 Å between NAG1 and NAG2 and 3.2 Å between NAG2 and NAG3). The O6 hydroxyl group of NAG1 forms a hydrogen bond with O3 of the NAG2 residue

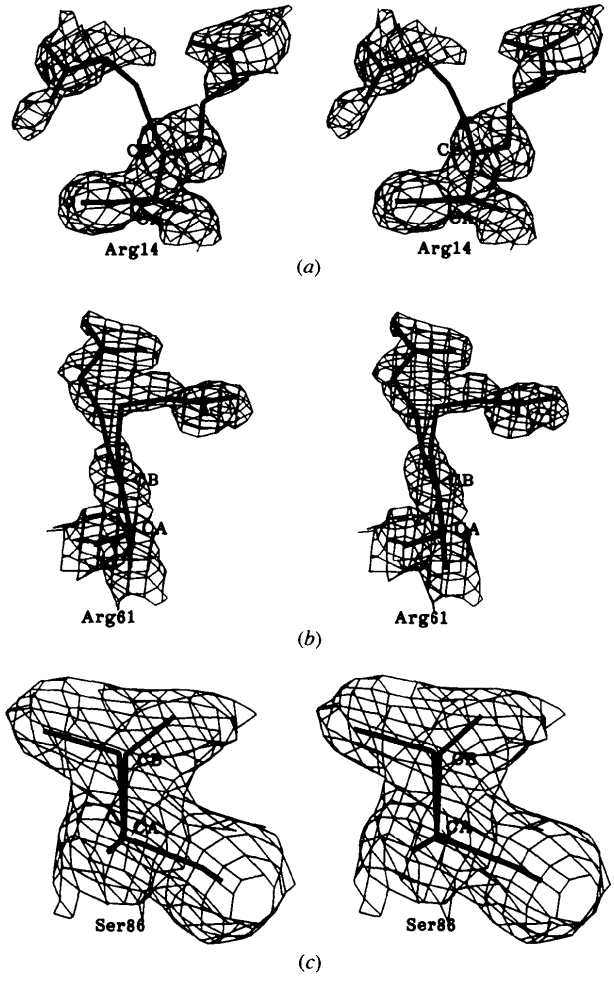

Fig. 2. Stereo drawings of the $2F_o - F_c$ electron density (1σ level) of disordered residues: (*a*) Arg14, (*b*) Arg61 and (*c*) Ser86.

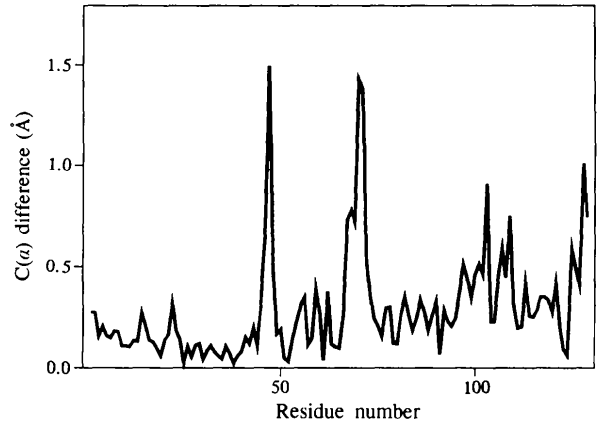

Fig. 3. Plot of C^{α} difference in TEL between the native structure and the $(GlcNac)_3$ complex after the least-squares superposition.

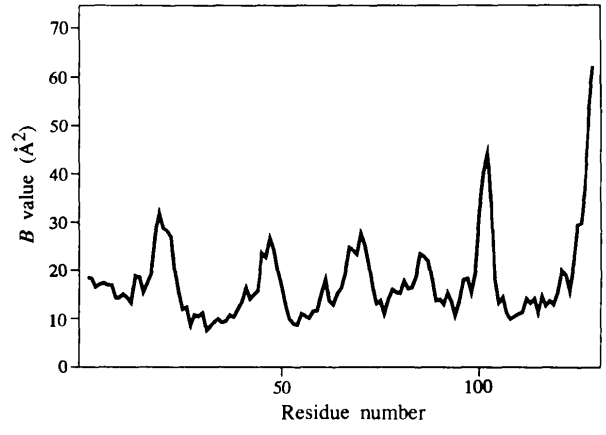

Fig. 4. Plot of average B values of the main-chain peptide groups.

with a distance of 3.3 Å, which stabilizes the (+)-*gauche* conformation of the C6—O6 bond. The average displacement parameters are 45.3, 18.5 and 14.4 Å^2 for NAG1, NAG2 and NAG3, respectively.

3.5. *TEL–(GlcNac)$_3$ interaction*

The (GlcNac)$_3$ molecule occupies the subsites *A*, *B* and *C* (Fig. 6). The NAG1 residue located at subsite *A* has no contact with TEL. The pyranose ring of the NAG2 residue is parallel to the indole moiety of Trp62 and in van der Waals contact. The NAG2 residue has no direct hydrogen-bonding contact with TEL, but the O6 hydroxyl group and the acetyl O atom form hydrogen bonds with three water molecules, one of which is hydrogen bonded to the side-chain group of Asn103. The O3 hydroxyl group is located within hydrogen-bonding distance of the O3 hydroxyl group of the twofold-symmetry-related NAG2 residue, while the amino group is hydrogen bonded to the sulfate ion. The acetyl O atom of the NAG3 residue bound to subsite *C* is hydrogen bonded to the main-chain N atom of Asn59, while the N atom attached to the acetyl group is linked to the peptide O atom of Ala107 *via* an N—H···O hydrogen bond. The O3 and O6 hydroxyl groups of the NAG3 residue form hydrogen bonds with the indolyl groups of Trp63 and Trp62, respectively.

Several water molecules participate in the stabilization of the (GlcNac)$_3$ molecule (Fig. 7). W197 forms hydrogen bonds with O6 and O7 of NAG2 and O3 of NAG3, which restrain the rotation of NAG2 and NAG3 around the glycosidic linkage. ND2 (Asn103) is linked to the acetyl O atom of NAG2 through W198 and W216, and NH2 (Arg112) is linked to the same O atom of NAG2 through W216. W177 links O6 of NAG3 to OD1(Asp48) and ND2(Asn59), while W183 forms hydrogen bonds with O1(NAG3) and O(Gln57).

3.6. *Crystal packing*

Two TEL molecules related by the twofold axis are arranged with their active-site clefts facing each other (Fig. 8). Short contacts are not found between the TEL molecules but a hydrogen-bonding contact is found between O3 hydroxyl groups of the two symmetry-related NAG2 residues, as described above. The sulfate ion is located on the twofold axis and forms many hydrogen bonds with TEL and (GlcNac)$_3$. The indolyl and guanidino groups of two symmetry-related TEL molecules are hydrogen bonded to the sulfate ion (Fig. 9). The average displacement parameter of 12.2 Å^2 indicates that the sulfate ion is tightly fixed in the cavity, isolated from bulk solvent.

4. Discussion

The sugar-binding model based on the structure of the HEL complex with (GlcNac)$_3$ has suggested the presence of six subsites, designated *A* to *F*, for the accommodation of substrate sugar residues (Blake *et al.*, 1967). The active centre is located between the subsites *D* and *E*. In the present TEL complex, the (GlcNac)$_3$ molecule occupies the subsites *A*, *B* and *C* and is bound in a similar manner as found in the structure of the HEL complex (Cheetham *et al.*, 1992). The same mode of binding is observed in the (GlcNac)$_3$ complex of partridge lysozyme (Turner & Howell, 1995), which differs in three amino-acid residues from HEL. However, the interaction of (GlcNac)$_3$ with TEL at the subsite *A* differs from those found in the complexes of hen and partridge lysozymes. In the HEL complex, Asn103 forms a hydrogen bond with O6 of the sugar residue at the subsite *A* and Asp101 is hydrogen bonded to O6 of the subsite *B*. On the other hand, Asp101 of partridge lysozyme forms hydrogen bonds with N2 at subsite *A* and O6 at subsite *B*, while Asn103 has no direct contact with (GlcNac)$_3$. In the TEL complex, the 101st residue is Gly, which has no contact with (GlcNac)$_3$. Asn103 is linked to O7 of NAG2 and O4 of NAG3 by water-mediated hydrogen-bond bridges. By the complex formation with (GlcNac)$_3$, the conformation of the 101–103 region changes, from the type I β-turn to the type III β-turn. Residue 103 is moved toward the sugar residue at subsite *B*. However, the side-chain group of the 103rd residue is oriented so as to avoid direct contact with the sugar residue. As a result, NAG1 has no contact with TEL and is highly flexible, as indicated by the relatively large *B* value of 45.3 Å^2. The corresponding sugar residue in the HEL complex is rotated around the glycosidic linkage to form hydrogen bonds with HEL (Fig. 10).

The pyranose ring of the NAG2 residue faces the indolyl group of Trp62 (Fig. 9). A similar hydrophobic contact has often been observed in the sugar complexes with chicken-type lysozymes. The C1—H, C3—H and C5—H bonds in the pyranose ring point toward the aromatic plane, with an attractive C—H···π interaction (Nishio, Umezawa, Hirota & Takeuchi, 1995). On the other side of the pyranose ring, three water molecules form hydrogen bonds with O5 and O6 of the NAG2 residue and O3 and O4 of the NAG3 residue. Turner & Howell (1995) have stressed the importance of the hydrogen-bond formation between Trp62 and O6 of NAG3 in the role of the indolyl group in inhibitor binding. In contrast, the importance of the planar side-chain group at this position has been demonstrated by enzymatic and crystallographic studies of several mutants of human lysozyme (Muraki, Harata & Jigami, 1992). The binding of the NAG2 and NAG3 residues to the TEL molecule is strengthened by the sulfate ion because the ion forms hydrogen bonds with the amino group of the NAG2 residue and O6 of the NAG3 residue. Such an enzyme–substrate contact mediated by an ionic solute molecule has not been observed in the sugar complexes of lysozymes. In the HEL complex, the *N*-acetyl group of

NAG2 has no contact with the protein molecule. On the other hand, the orientation of the *N*-acetyl group of NAG2 in the TEL complex is restricted by the formation of the hydrogen bond between the amino group and the sulfate ion.

To compare the binding of $(GlcNac)_3$ in the TEL and HEL complexes, the structures of the TEL and HEL complexes were superimposed by least-squares superposition of equivalent C^{α} atoms. The $(GlcNac)_3$ structures in both complexes are shown in Fig. 10. The binding mode of the NAG3 residue is nearly identical to that in the complexes of HEL and partridge lysozymes. Four hydrogen bonds between NAG3 and the protein have been observed in the $(GlcNac)_3$ complexes of these three lysozymes. The subsite *C* is highly specific to the structure of GlcNac. The *N*-acetyl group of the NAG3 residue in the TEL–$(GlcNac)_3$ complex is recognized by the protein, with the formation of hydrogen bonds to O(Ala107) and N(Asn59), and links two lobes of the active-site cleft. A similar hydrogen-bond bridge has been observed in the HEL complex with *N*-acetylmuraminyl-*N*-acetylglucosaminyl-*N*-acetylmuraminic acid (Strynadka & James, 1991), in which the GlcNac moiety is bound to the subsite *C*.

The binding of $(GlcNac)_3$ makes the cleft narrower. The difference distance map (Fig. 11) clearly indicates the movement of two lobes of the cleft upon the binding of $(GlcNac)_3$. Residue 103 moved by 1.0–1.5 Å toward the region of residues 59–80. The residues 68–71 moved by 0.5–1.5 Å toward the region of residues 101–120. The regions of residues 50–80 and 100–120, which correspond to the regions of the two lobes of the cleft, became

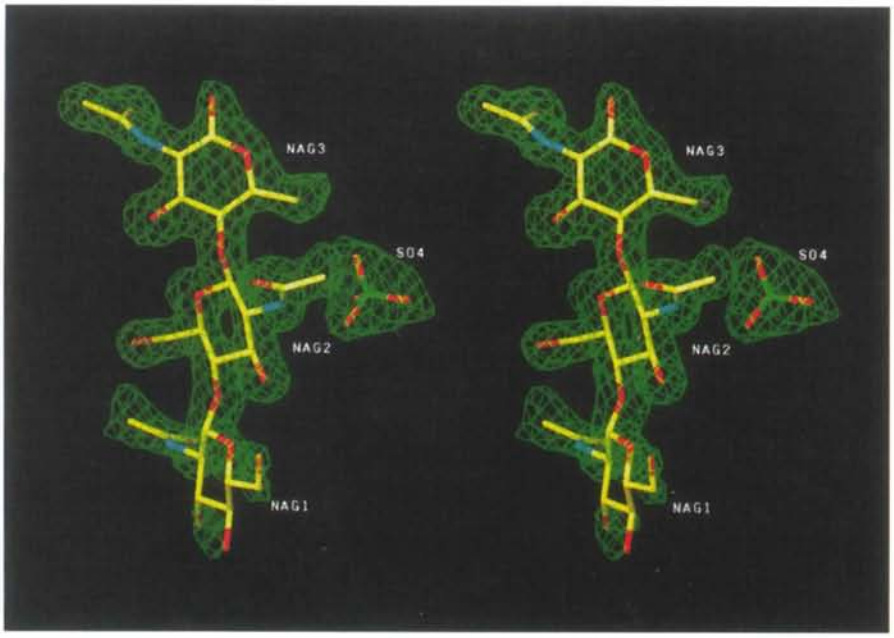

Fig. 5. Stereo drawing of the $2F_o - F_c$ electron density (1σ level) of the $(GlcNac)_3$ molecule and sulfate ion.

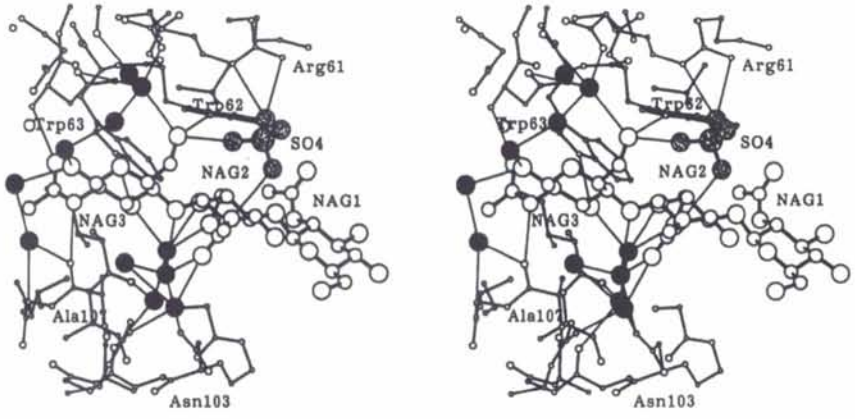

Fig. 6. Stereo drawing of the $(GlcNac)_3$ molecule bound to the active site of TEL. The sulfate ion is shaded and water molecules are shown with full circles. Thin lines denote possible hydrogen-bonding contacts.

closer by 0.5–1.0 Å. In contrast, the loop region of residues 45–48 connecting two β-strands moved away from the cleft. A similar structural change was observed in the TEL complex with $(GlcNac)_2$, although the $(GlcNac)_2$ is bound in a different manner (Harata & Muraki, 1995). The intermolecular contacts involve Asp48, Gly67 and Arg68. The conformation of the regions including these residues may be affected by the crystal packing and the intermolecular contacts may stabilize these local structures.

The lack of direct contact between TEL and sugar residues at subsite *A* affects the catalysis of the hydrolysis of oligosaccharides. In the lysozyme-catalyzed hydrolysis of $(GlcNac)_5$, HEL produces GlcNac as the major

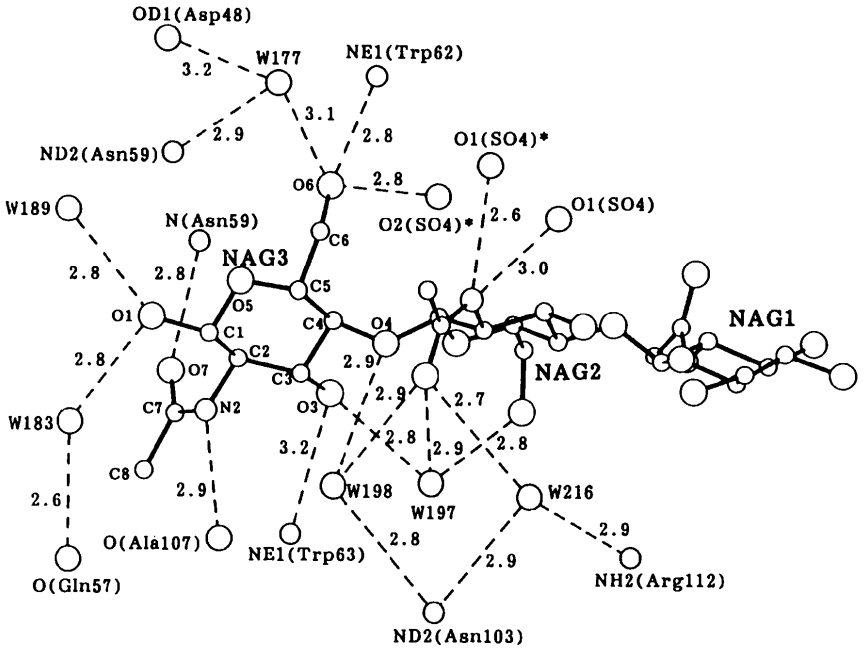

Fig. 7. Schematic drawing of the interaction of $(GlcNac)_3$ with TEL and the sulfate ion. The numbering of the pyranose ring is shown in the NAG3 residue. An asterisk indicates the residue in the two-fold-symmetry-related molecule.

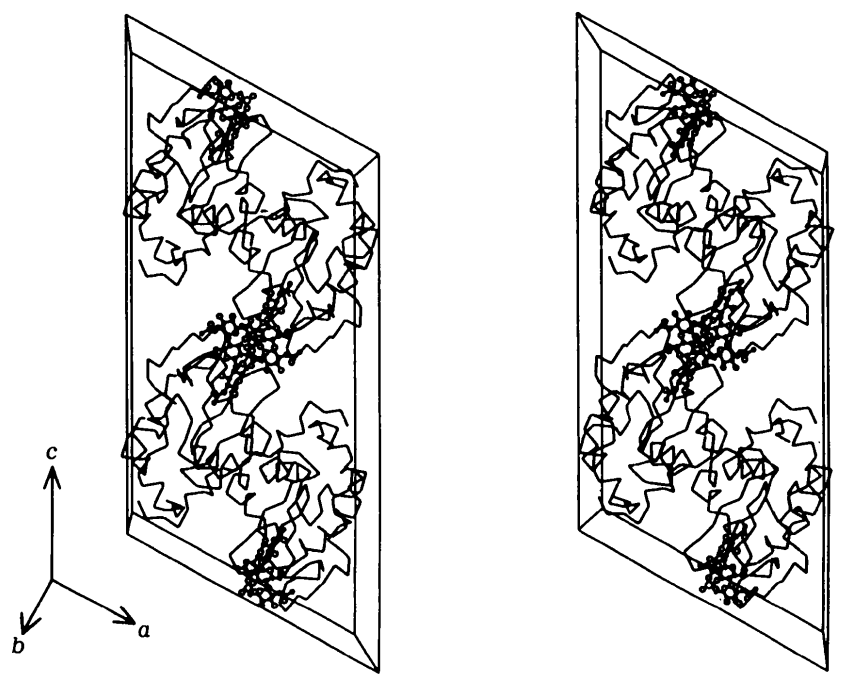

Fig. 8. Stereo drawing of the crystal packing viewed along the *b* axis. Atoms in $(GleNac)_3$ and the sulfate ion are shown with circles.

product, whereas $(GlcNac)_2$ is the most abundant product in the TEL-catalyzed hydrolysis (Fukamizo *et al.*, 1983). This suggests that HEL preferably binds the $(GlcNac)_5$ at the subsites *A–E*, while TEL would rather accommodate the sugar molecule at the subsites *B* to *F*. The important role of residue 101 in the binding of the sugar at subsite *A* has been demonstrated by the chemical modification of Asp101 of HEL (Fukamizo *et al.*, 1986). The modification of the carboxyl group of Asp101 by the introduction of ethanolamine or glucosamine decreased the sugar-binding ability. Moreover, the cleavage pattern of $(GlcNac)_5$ has suggested that the sugar occupies the subsites *B–F* of the modified HEL.

We tried to prepare the crystalline complex of TEL with $(GlcNac)_4$ by co-crystallization. However, only GlcNac was found in the crystal structure, suggesting that $(GlcNac)_4$ was hydrolyzed during the crystallization (Harata *et al.*, unpublished work). For the hydrolysis reaction, TEL requires the binding of $(GlcNac)_4$ at the subsites *B–E* or *C–F*. Being different from TEL, human lysozyme forms a crystalline complex with $(GlcNac)_4$, which occupies the subsites *A–D* (Song, Inaka, Maenaka & Matsushima, 1994). The sugar residue located at subsite *A* has no direct contact with the protein molecule. In another crystal of the complex with $(GlcNac)_4$, prepared in the presence of $(GlcNac)_6$, the hydrogen-bonding contact of the *N*-acetyl group of the sugar residue at subsite *A* with Asp102, which corresponds to Asp101 of HEL, was observed in only one of the two independent molecules (Song *et al.*, 1994). The weak binding ability of subsite *A* is considered to be related to the catalytic properties observed in the hydrolysis of $(GlcNac)_5$. Being similar to TEL, human lysozyme mainly produces $(GlcNac)_2$ in the hydrolysis of $(GlcNac)_5$ (Muraki, Morikawa, Jigami & Tanaka, 1989). The subsite *A* is far from the active centre. However, the results suggest that the structure and sugar-binding ability of subsite *A* are responsible for the product distribution in the catalytic reaction with oligosaccharides.

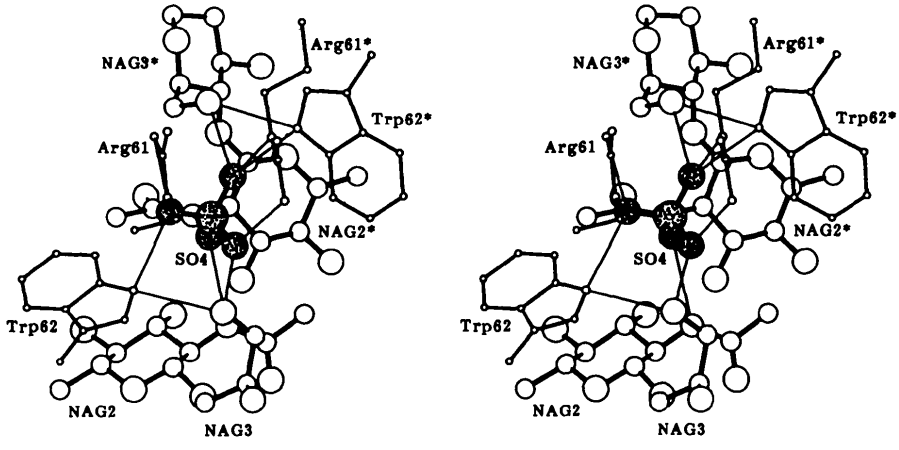

Fig. 9. Stereo drawing of the interaction of the sulfate ion with TEL and $(GlcNac)_3$. An asterisk indicates the residue in the twofold-symmetry-related molecule. Possible hydrogen-bonding contacts are shown with thin lines. The twofold-symmetry-related mate of the sulfate ion is not shown for clarity.

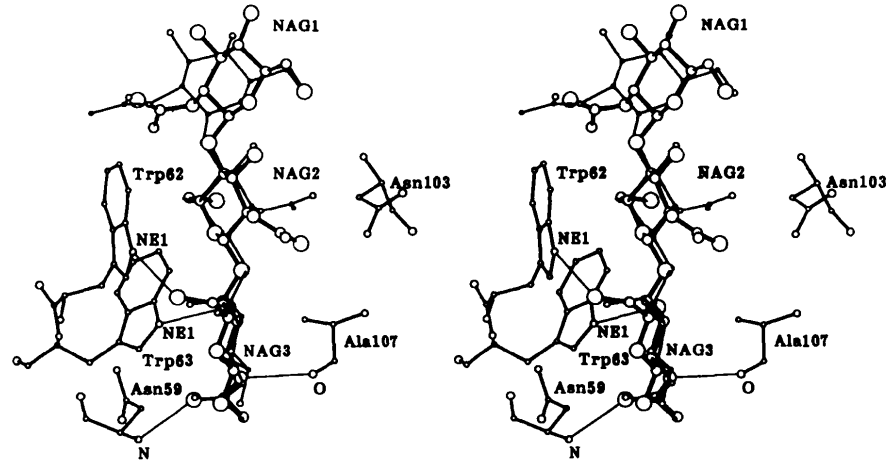

Fig. 10. Stereo drawing of the $(GlcNac)_3$ molecule in the active-site cleft. The $(GlcNac)_3$ molecule in the HEL complex (Cheetham *et al.*, 1992) is shown with small circles after the least-squares superposition of the TEL and HEL complexes for equivalent C^{α} atoms. Hydrogen-bonding contacts of $(GlcNac)_3$ with some amino-acid residues in TEL are shown with thin lines.

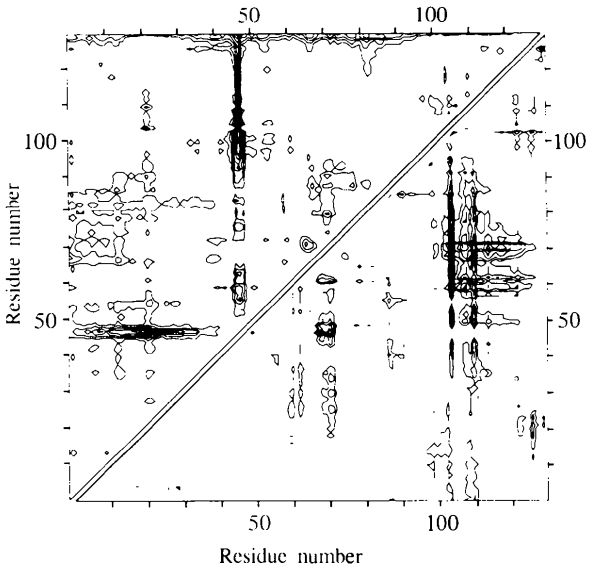

Fig. 11. Difference distance map for C^{α} atoms in TEL between the native structure and the $(GlcNac)_3$ complex. The difference $C^{\alpha}\cdots C^{\alpha}$ distances, Δr_{ij}[$(GlcNac)_3$ complex] - Δr_{ij}(native TEL), are plotted. Contours are drawn at 0.2, 0.4, 0.6 Å (top left) and −0.2, −0.4, −0.6 Å (bottom right).

References

Arnheim, N., Millett, F. & Raftery, M. A. (1974). *Arch. Biochem. Biophys.* **165**, 281–287.

Banerjee, S. K. & Rupley, J. A. (1975). *J. Biol. Chem.* **250**, 8267–8274.

Blake, C. C. F., Johnson, L. N., Mair. G. A., North, A. C. T., Phillips, D. C. & Sarma, V. (1967). *Proc. R. Soc. London Ser. B*, **167**, 378–388.

Bott, R. & Sarma, R. (1976). *J. Mol. Biol.* **106**, 1037–1046.

Brünger, A. T. (1992). *X-PLOR. Version 3.1. A System for X-ray Crystallography & NMR*, pp. 233–270. New Haven: Yale University Press.

Brünger, A. T., Kuriyan, J. & Karplus, M. (1987). *Science*, **235**, 458–460.

Cheetham, J. C., Artymiuk, P. J. & Phillips, D. C. (1992). *J. Mol. Biol.* **224**, 613–628.

Fukamizo, T., Hayashi, K. & Goto, S. (1986). *Eur. J. Biochem.* **158**, 463–467.

Fukamizo, T., Torikata, T., Nagayama, T., Minematsu, T. & Hayashi, K. (1983). *J. Biochem.* **94**, 115–122.

Harata, K. (1993). *Acta Cryst.* D**49**, 497–504.

Harata, K. & Muraki, M. (1995). *Acta Cryst.* D**51**, 718–724.

Howell, P. L., Almo, S. A., Persons, M. R., Hajdu, J. & Petsko, G. A. (1992). *Acta Cryst.* B**48**, 200–207.

Kraulis, P. J. (1991). *J. Appl. Cryst.* **24**, 946–950.

LaRue, J. N. & Speck, J. C. Jr (1970). *J. Biol. Chem.* **245**, 1985–1991.

Luzzati, V. (1952). *Acta Cryst.* **5**, 802–807.

Mo, F. & Jensen, L. H. (1978). *Acta Cryst.* B**34**, 1562–1569.

Muraki, M., Harata, K. & Jigami, Y. (1992). *Biochemistry*, **31**, 9212–9219.

Muraki, M., Morikawa, M., Jigami, Y. & Tanaka, H. (1989). *Eur. J. Biochem.* **179**, 573–579.

Nishio, M., Umezawa, Y., Hirota, M. & Tekeuchi, Y. (1995). *Tetrahedron*, **51**, 8665–8701.

Song, H., Inaka, K., Maenaka, K. & Matsushima, M. (1994). *J. Mol. Biol.* **244**, 522–540.

Strynadka, N. C. J. & James, M. N. G. (1991). *J. Mol. Biol.* **220**, 401–424.

Turner, M. A. & Howell, P. L. (1995). *Protein Sci.* **4**, 442–449.